Copper Nanowire-Based Aerogel with Tunable Pore Structure and Its Application as Flexible Pressure Sensor

Xiaojuan Xu,[†,‡] Ranran Wang,*[,†] Pu Nie,[†,‡] Yin Cheng,[†,‡] Xiaoyu Lu,[†,‡] Liangjing Shi,[†] and Jing Sun*[,†]

[†]State Key Laboratory of High Performance Ceramics and Superfine Microstructure, Shanghai Institute of Ceramics, Chinese Academy of Sciences, 1295 Ding Xi Road, Shanghai 200050, P. R. China

[‡]University of Chinese Academy of Sciences, 19 Yuquan Road, Beijing 100049, P. R. China

Ⓢ Supporting Information

ABSTRACT: Aerogel is a kind of material with high porosity and low density. However, the research on metal-based aerogel with good conductivity is quite limited, which hinders its usage in electronic devices, such as flexible pressure sensors. In this work, we successfully fabricate copper nanowire (CuNW) based aerogel through a one-pot method, and the dynamics for the assembly of CuNWs into hydrogel is intensively investigated. The "bubble controlled assembly" mechanism is put forward for the first time, according to which tunable pore structures and densities ($4.3-7.5$ mg cm^{-3}) of the nanowire aerogel is achieved. Subsequently, ultralight flexible pressure sensors with tunable sensitivities (0.02 kPa^{-1} to 0.7 kPa^{-1}) are fabricated from the Cu NWs aerogels, and the negative correlation behavior of the sensitivity to the density of the aerogel sensors is disclosed systematically. This work provides a versatile strategy for the fabrication of nanowire-based aerogels, which greatly broadens their application potential.

KEYWORDS: one-pot method, copper nanowires, aerogel, piezoresistivity, tunable density
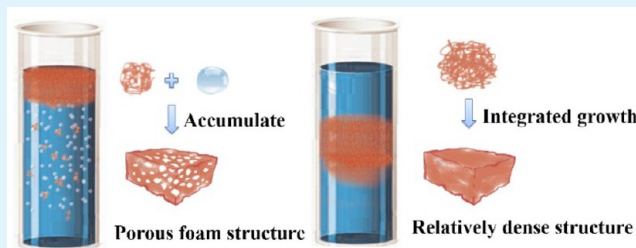
1. INTRODUCTION

Aerogel is a porous solid material, with the cavities in the three-dimensional network filled with gas in place of liquid.[1] At present, the research on aerogel mainly focused on types of silica,[2−4] metal oxides,[5,6] organic compounds[7,8] and carbon-based materials.[9−11] Because of a number of unique properties, such as extremely low density, high porosity, and specific surface area,[12] aerogel materials hold tremendous application prospects in the fields of insulation materials,[13,14] super-capacitors,[15−17] optical lightweight optics,[18] and flexible sensors.[19−21] Recently, aerogels have started to be adopted as pressure sensors extensively because of their good electrical conductivity, excellent mechanical properties, and this ultralow density, which can reduce the overall weight of electronic equipment.[20,22] The current research on aerogel sensors mainly focused on the materials of graphene,[23−26] carbon nanotubes,[27] and metal nanowires.[20,22,28] CuNW aerogel monolith can be a good candidate for piezoresistive pressure sensor, for the applied pressure induced geometry change of the aerogel structure can effectively lead to corresponding electrical resistance change.[29] Specifically, the compression on the unit pores of the aerogel directly causes more intimate contact in between nanowires, thus decreasing the contact resistance. Also worth noting is that the self-assembly method for aerogel preparation is suitable for large-scale production, which paves the way for their practical and pervasive applications.

However, metal-based aerogels are rarely reported. Though alkoxide precursor method,[30,31] as the primary and well-developed preparation strategy, achieved considerable progress, there still leaves some limitations, especially for the fabrication of metal aerogels, due to the lack of appropriate precursor. Despite that, metallic nanowires can be harnessed as building blocks of metal-based aerogels owing to the high aspect ratio, as the Doi and Edwards theory indicates that rodlike molecules are prone to entanglement and self-assembly, resulting in sols at proper concentrations.[32−34] As a metal element with excellent electrical conductivity and abundant reserves, CuNWs have natural advantages for the fabrication of metal aerogel.[35] However, either the mechanism investigation or the tunable preparation of copper nanowire aerogels still lags far behind other aerogel materials, so far. In this context, to develop a facile and tunable preparation method for copper nanowire aerogel is of great significance from both science and engineering application perspectives.

On the basis of the above concerns, we intensively studied the fabrication process of CuNW aerogel and applied it as a pressure sensor. CuNW aerogels were freeze-dried from CuNW hydrogels. CuNW hydrogels were obtained through a one-pot method in which CuNWs were synthesized by reduction and meanwhile self-assembled into the sol flocs. During the one-pot synthesis, CuNWs grew into initial sol flocs and subsequently floated upward to aqueous surface, where CuNW hydrogel was

formed, by a large number of generated bubbles. Considering the important influences of bubbles on the final CuNW hydrogel structure, we proposed a formation mechanism named "bubble controlled assembly". By tuning the reaction parameters, we successfully realized the fabrication of aerogels with tunable pore structure and density, ranging from 4.3 mg cm^{-3} to 7.5 mg cm^{-3}. Our research provided a simple and controllable method for the CuNW aerogel synthesis, and also served as a reference for other metal nanowires aerogels. The synthesized aerogel monoliths were employed as flexible pressure sensors which proved to possess good mechanical and sensing properties. Moreover, we confirmed that the pore structure and density had great influence on the performance of the sensors, in which the density has a negative correlation to the sensor sensitive and detection limit. The sensitivity could be tuned from 0.02 kPa^{-1} to 0.7 kPa^{-1} via pore structure adjustment, which highlighted the importance of the mechanism understanding and morphology control.

2. RESULTS AND DISCUSSION

The preparation process of CuNW aerogel monolith is illustrated in Figure 1. First, copper sulfate ($CuSO_4$) was
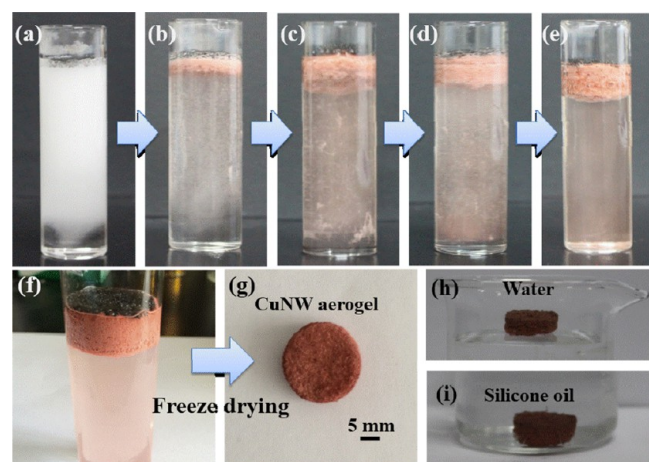

Figure 1. CuNW hydrogel/aerogel production process. (a–e) The one-pot production of Cu hydrogel: the growth of nanowires, the self-assembly of sol flocs and the stacking of hydrogel; (f) prepared CuNW hydrogel; (g) The aerogel after freeze-drying; (h, i) The CuNW aerogel floating in the water and sinking in the silicone oil.

mixed with hydrazine and ethylenediamine (EDA) in high concentration of sodium hydroxide (NaOH).[34,36] The above solution was sonicated and bubbles originated from sonication were trapped within the viscous solution caused by concentrated NaOH. The homogeneous solution appeared milky white due to the presence of numerous bubbles. Then the solution was transferred to a flat-bottomed tube with a piece of polyurethane (PU) foam placed on top of the liquid surface, which helped to insulate the CuNW sols from the ambient air so as to avoid oxidation (Figure S1). Finally, the tube was heated in oil bath at temperature of 80 °C for 1 h. Figure 1a–e show the fabrication process of CuNW hydrogel, which contains five stages: (i) When the tube was put into the oil bath, the elevated temperature lowered the viscosity of the solution which released the trapped bubbles and made the milky white solution clear (Figure 1a); (ii) After about 25 min, red sol flocs began to appear in the solution. The flocs floated upward with surrounded bubbles to the surface and stacked to a bulk beneath the PU foam. In this process the bubble concentration deceased but the solution turned turbid on account of generated CuNWs (Figure 1b); (iii) As the concentration of bubbles in the solution decreased further, the size of upward-floating sol flocs became larger and stacked to form the main body of CuNW hydrogel monolith (Figure 1c); (iv) After about 45 min, as the result of the consumption of the reaction reagents, the size of the upward-floating flocs became small and the amount decreased (Figure 1d); (v) growth of CuNW stopped after about 1 h with the solution turning clear, and a bright red CuNW hydrogel monolith with the same shape of vessel was obtained (Figure 1e). After the fabrication the hydrogel monolith was washed by 5% hydrazine for several times to protect it from oxidation, followed by a freeze-drying process as illustrated in Figure 1f, g. Freeze-drying helped to maintain the three-dimensional porous structure. The as-produced CuNW aerogel showed a typically cylindrical shape with low density (6.3 mg cm^{-3}) and high porosity (99.9%). The aerogel monolith floated on but did not absorb water (Figure 1h), whereas it was totally submerged when transferred to the silicone oil (Figure 1i). It indicates that the CuNW aerogel has superhydrophobic surfaces for selective uptake of oil. Because of their surface superhydrophobicity and extra high porosity (>99.9%), aerogels have the potential to remove oils or nonpolar organic solvents from water without adsorption of water.
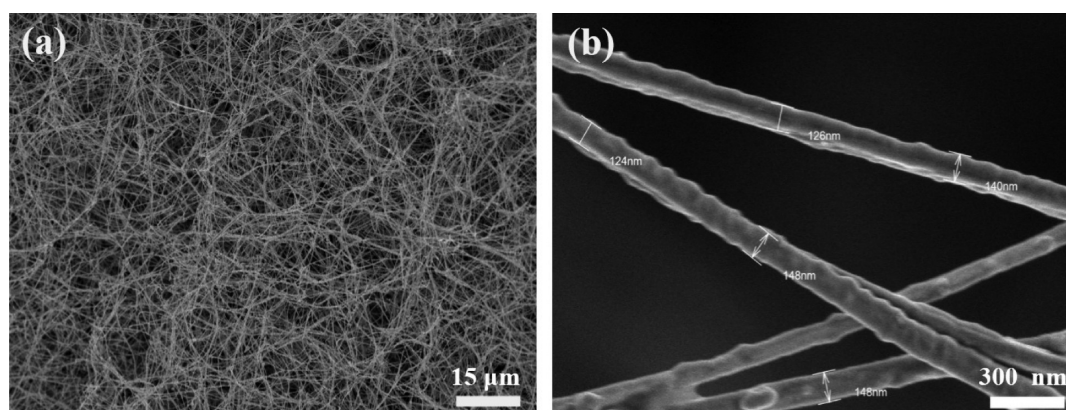

Figure 2. SEM images of the CuNW aerogel with different magnifications: (a) low magnifications; (b) high magnifications showing the nanowire network structure and single nanowire morphology.
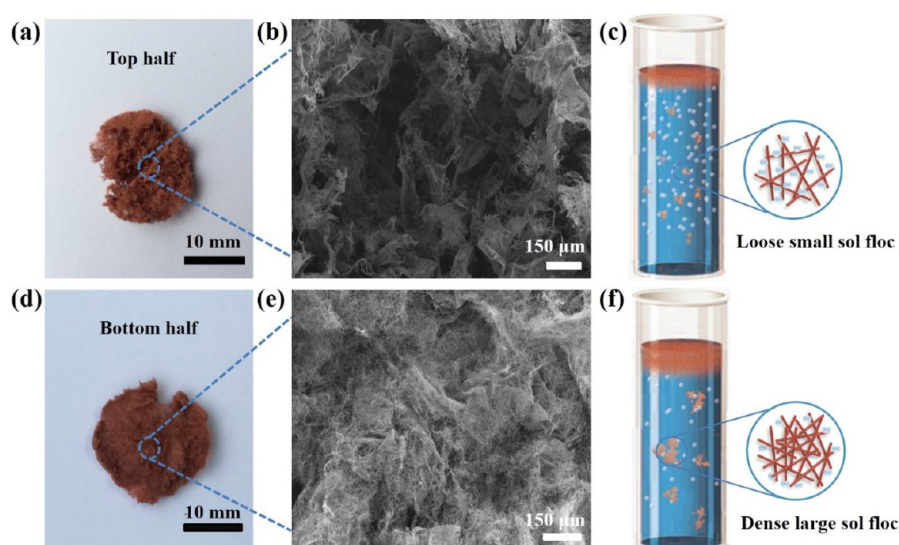
Figure 3. Hierarchical internal microstructure of the mixed CuNW aerogel and different fabrication manner: (a) the digital photograph and (b) SEM image for the top half of the mixed structure CuNW aerogel; (c) the illustration of the formation procedure of the top half; (d) the digital photograph and (e) SEM image for the bottom half of the mixed structure CuNW aerogel; (f) the illustration of the formation procedure of the bottom half.

Figure 2a exhibited the highly porous network of the CuNW aerogel. The nanowires spontaneously formed a three-dimensional network without need of additional binding agent. Further SEM observation indicated that these nanowires had uniform size and the average diameter of the nanowires was ∼130 nm as calculated from 50 nanowires randomly selected from the SEM images (Figure 2b). Because the fabrication process involved no organic polymers, the surface of the nanowire appeared very clean. The Xray diffraction (XRD) pattern was then recorded (Figure S2). The peaks at $2\theta = 43.3$, 50.4, and 74.2° correspond to the diffractions from the (111), (200), (220) crystalline planes of Cu (JCPDS #04−0836). No additional peaks relating with CuO or C were observed, indicating the high chemical purity of these NWs.

To further explore the internal structure of the CuNW aerogel monolith, the aerogel was torn off and characterized by SEM. It was found that the monolith possessed a mixed structure. The top part of the aerogel showed a porous structure, while the bottom part appeared much denser, as compared in Figure 3a,d. The morphology characterization in Figure 3b, e clearly confirmed the structure contrast: the top part displayed a structure with high pore density, and the nanowires in the bottom stacked far more tightly as a comparison. To unravel the morphology difference of the aerogel from top to bottom, we should first understand the step-by-step process in forming a CuNW hydrogel monolith, which comprised the synthesis of CuNWs, self-assembly of CuNWs into the sol flocs and the stacking of the flocs into a hydrogel monolith, successively. This unique formation process resulted in a CuNW based hydrogel with hierarchical structure. The synthesis of CuNWs in this work was based on the one-pot method and the specific chemical reaction is as follows eq 1. In this process, the cupric ions were reduced to form CuNWs, during which nitrogen gas was also generated to increase bubble concentration within the reaction solution.

$$Cu^{2+} + N_2H_4 + 4OH^- \rightarrow 2Cu + N_2 + H_2O \qquad (1)$$

For the sol formation, it is according to the Doi and Edwards theory which describes the phase behavior of a suspension of rodlike molecules, The concentration of CuNWs could be described through the volume fraction φ, which was defined as[33]

$$\varphi = \frac{\pi n L d^2}{4} = \frac{\pi n L^3}{4 a_r^2} \qquad (2)$$

In this equation, n is the number of CuNWs per unit volume, L is the length of each nanowire, d is the diameter, and a_r (L/d) referred to the corresponding aspect ratio. When $n = 1/(dL^2)$, the volume fraction $\varphi = a_r^{-1}$. At this time, the concentration of nanowires in the solution reached the critical state, thus the theoretical gel formation concentration can be defined as $\varphi_{sol} = a_r^{-1}$. The synthesis of CuNWs was very rapid which resulted in the fast increase of nanowires concentration in solution. When the concentration in the solution reached the sol formation concentration (i.e., the critical state), the movement of CuNWs caused a high probability to meet another one. Because of the van der Waals forces, the nanowires contact with each other and with the quantity of connected nanowires increase, a 3D continuous nanowires network can be formed. Finally, the formation of the sol flocs in the solution floated upward to the surface driven by the bubbles, and stacked into the hydrogel monolith under the PU foam.

On the basis of the above observation, a mechanism called "bubble controlled assembly" was proposed to explain the formation of the hydrogel. The bubbles in the solution came from two aspects: generated from the sonication of hydrazine and the reduction reaction according to eq 1. Before reaction, both the high concentration of NaOH and the relatively low temperature led to a high viscosity of the solution. As a result, numerous bubbles generated by the sonication of hydrazine were trapped in the solution which resulted in a uniform milky white solution. When it was heated in the oil bath, as the temperature rose, the viscosity of the solution decreased, so the trapped bubbles began to float upward. At the same time, CuNWs started to form and self-assembled to form sol flocs.
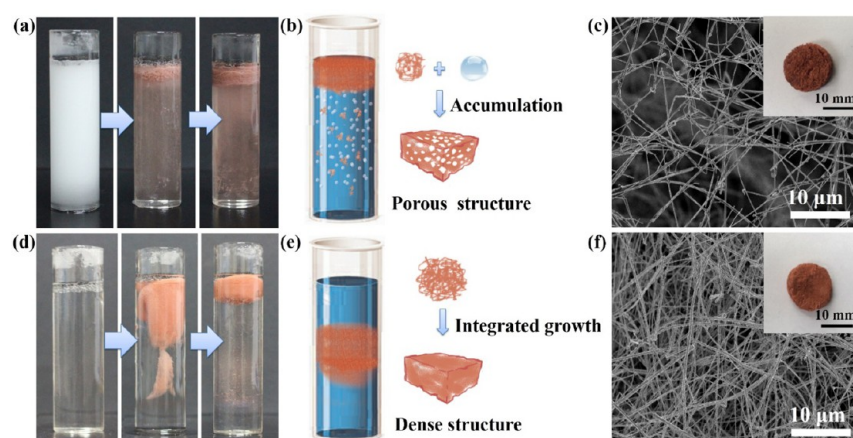
Figure 4. Controlled fabrication of CuNW aerogel with different structures. (a) The digital photographs and (b) illustration of the fabrication manner for porous CuNW aerogel; (c) SEM image of the as-prepared porous CuNW aerogel and the final product shown in the inset of c; (d) digital photographs and (e) illustration of the fabrication manner for dense CuNW aerogel; (f) SEM image of the as-prepared dense CuNW aerogel and the final product shown in the inset of f.

Due to the presence of numerous bubbles, the density of generated sol flocs was very low and the buoyancy force was large. Resultantly, the sol flocs would float upward to the surface before growing into a large-volume bulk. Lastly, the floating-upward flocs and bubbles stacked under the PU foam to form a bubble-rich structure, as showed in Figure 3c. As the reaction continued, the bubble concentration decreased, and as a result, the sol flocs could grow larger before floating upward. Figure 3f showed the fabrication mode of bottom half, in which large-volume flocs stacked to form the hydrogel monolith with less bubbles. The absence of bubbles and large-volume flocs gave rise to a dense structure showed in Figure 3d. In general, the varying bubble concentration during the CuNW hydrogel fabrication process determined the size of single sol floc and the stacking manner of the monolith, which affected the final pore structure of the aerogel monolith.

According to the mechanism mentioned above, the bubble concentration at the beginning of the reaction and the rate of bubble generation during the reaction determined the size of the upward floating sol flocs and the stacking manner of the hydrogel monolith. By tuning the reaction parameters such as concentration of reactants and heating temperature, we could adjust the bubble concentration during different reaction stages, which influenced the final morphology of the aerogel monolith. Regarding this as a guide, we have successfully prepared CuNW aerogels with homogeneous porous and dense structure.

To obtain the porous CuNW aerogel monolith, we increased the concentration of the $CuSO_4$, EDA, and hydrazine as listed in Table S1 and the heating temperature was also increased from 80 to 90 °C. Figure 4a illustrates the preparation process of such porous CuNW hydrogel monolith after reaction parameters adjustment. The increase of reagents concentration and temperature resulted in accelerated reaction rate. On the one hand, the accelerated reaction enabled the concentration of the CuNWs in solution to reach the gel formation concentration within a short time before original bubbles escaped. On the other hand, due to the increase of hydrazine concentration and the reaction rate, the assembly of sol flocs was accompanied by the presence of numerous bubbles. As a result, the CuNW sol flocs could float upward to the surface controlled by the buoyancy of the bubbles before growing into a large volume bulk. Finally, the as-prepared hydrogel monolith

was generated through the stacking of the small sol flocs and bubbles, which resembled a sponge-like structure (Figure 4b). A low-magnification SEM image of the aerogel after freeze-drying shown in Figure 4c revealed a sparse nanowire network and high porosity. The inset in Figure 4c demonstrated the aerogel with a porous surface which corresponded to the observation of the microstructure.

To obtain the aerogel monolith with dense structure, we adopted another set of parameters for the preparation (Table S1). The concentration of NaOH was reduced by half to lower the viscosity of the solution, thus deterring the trapping of bubbles within the solution. Meanwhile, the concentration of $CuSO_4$, EDA and hydrazine were also reduced by half respectively and the temperature was decreased from 80 to 70 °C. These adjustments aimed at reducing the bubble concentration before reaction while slowing down the rate of bubble generation. Figure 4d illustrated a completely different fabrication process compared with Figure 4a. Through observation we found that at the beginning of the reaction, the solution appeared clear, indicating the absence of bubbles in the solution. The bubbles, which controlled the upward-floating of the CuNW sol flocs, came only from the reduction reaction. The CuNWs assembled into sol flocs through van der Waals force, and the flocs could grow into a large-volume bulk before floating up controlled by enough bubbles. The fabrication manner of hydrogel monolith is showed in Figure 4e which corresponds to a relatively dense structure aerogel monolith after freeze-drying. The inset of Figure 4f demonstrated the aerogel monolith with dense surface, in which no obvious pores are observed. A low-magnification SEM image (Figure 4f) also revealed its microstructure. The network density was larger and there are no obvious macro-pores in the material in comparison with Figure 4c. The electrical conductivity of the aerogels with varying pore structure and density was measured, which proved to be highly related to the density value aerogels with higher density (4.3−7.5 mg cm^{-3}) possessed higher conductivity (1.6−12.8 S cm^{-1}), as seen in Table S1. In summary, we presented a simple and feasible method to realize the synthesis of CuNW aerogel with controlled density (Table S1) and pore structure.

The synthesized CuNW aerogel monolith was expected to be an ideal sensing material as piezoresistive sensors due to the
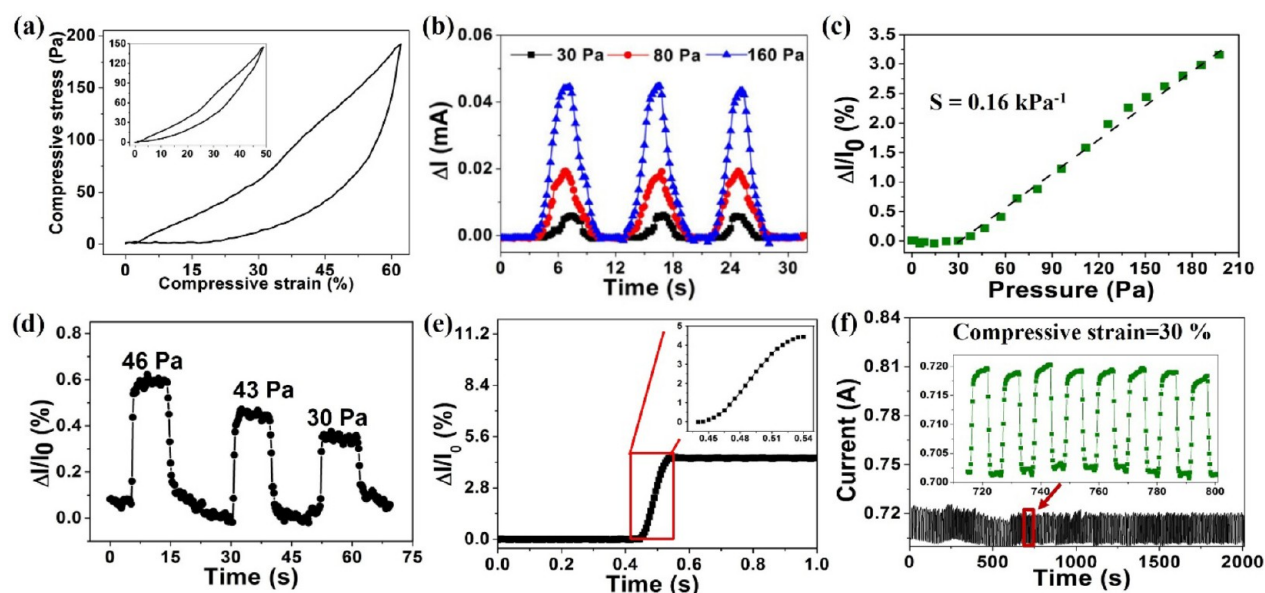
Figure 5. Mechanical and sensor performance of the mixed structure CuNW aerogel: (a) Compressive stress strain curves of aerogels at the compressive strain of 60% and at the compressive strain of 50% in the inset of a. (b) Multiple-cycle tests of repeated loading and unloading pressure ranging from 30 to 160 Pa. (c) Pressure−response curves for CuNW aerogel. (d) Current variation of CuNW aerogel when step pressures (46, 43, and 30 Pa) were applied to determine the detection limit. (e) Real-time current variation when a rubber cubic was dropped from above (~1 mm) the center of a sensing pixel. The inset shows the close-up of the signal response part. (f) Durability test of the CuNW aerogel. Relative current variation at compressive strain of 30% up to 200 loading cycles.
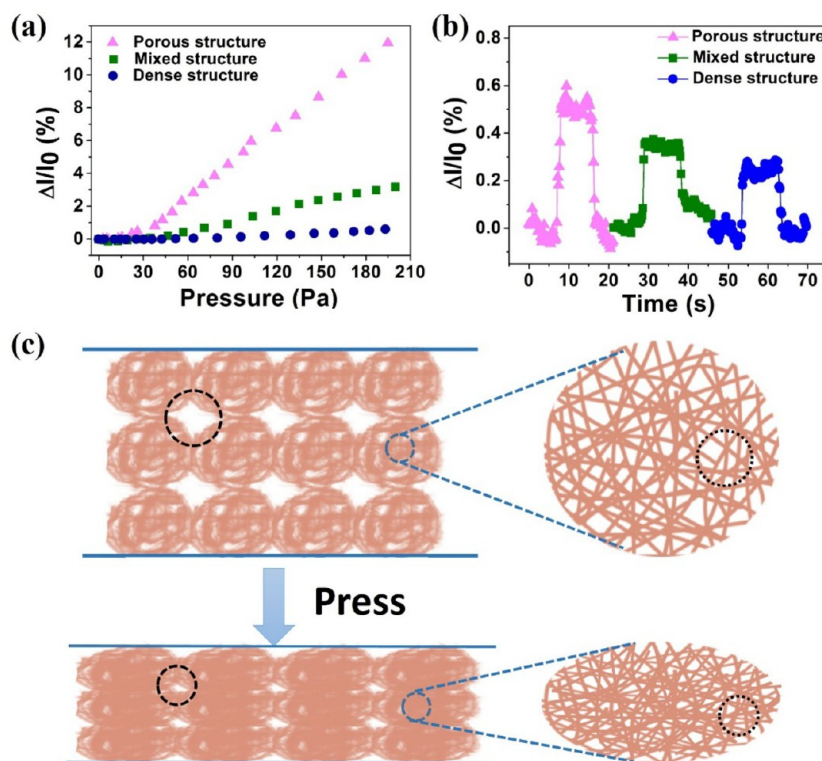

Figure 6. (a) Pressure−response curves for porous structure aerogel, mixed structure aerogel and dense structure aerogel, respectively; (b) current variation of CuNW aerogel with different structure (porous, mixed, dense structure) when step pressures (14, 30, and 43 Pa) were applied to determine the detection limit; (c) illustration of the pore structure of the CuNW aerogel variation before and after press.

high conductivity combined with good mechanical compliance of the CuNWs. Besides, the extraordinary flexibility of the CuNW aerogel could allow large deformations without fracture. The inset of Figure 5a demonstrated a CuNW aerogel which could almost recovered to its original height after a loading-

releasing cycle of strain up to 50%. Figure 5a showed the compressive and recovery stress versus stain curve of the as-produced aerogel at the compressive strain of 60%, where two regions of deformation could be observed: nearly linear region at $\varepsilon < 40\%$ and a following densification region.

To measure its electrical and sensing properties, the synthesized CuNW aerogel monolith was assembled into a resistive-type pressure sensor by sandwiching the monolith on top of a nickel tablet and beneath an ultralight aluminum foil with two copper wires connected to each electrode (Figure S3). Under a constant direct voltage, the current signal of the sensor was recorded with the increase of pressure imposed perpendicularly on the surface of the aluminum foil. The relative current variation ($\Delta I/I_0 = (I_P - I_0)/I_0$, ($I_P$ and I_0 denote the current with and without applied pressure, respectively) was calculated, which corresponded to the resistance variation of the aerogel sensor. On the basis of measured values and the quantitative pressure-induced current changes, it could be seen that the different pressures lead to different but stable current change signals (Figure 5b). The sensitivity of our aerogel sensor can be defined as $S = \delta(\Delta I/I_0)/\delta P$ (δP is the applied pressure). In Figure 5c, the response curve in the pressure sensing range kept an almost linear increasing trend, with the sensitivity of 0.16 kPa^{-1}. The device is more sensitive than the previous CuNW aerogel monolith sensor reported (0.036 kPa^{-1})[22] and our device do not require expensive materials or complex microfabrication tools for aerogel sensor preparation. As shown in Figure 5d, a detection limit of 30 Pa was obtained by inputting ultralow step pressures on the device. To determine the response time of pressure sensing, we input a quasi-transient step pressure (5%) and recorded the real-time (time resolution of 5 ms) signal response. The response time was captured to be as fast as ~80 ms (Figure 5e), which allowed the monitoring of vast majority of human motions. To test the reproducibility of the response signal, we input consecutive step pressures of 200 cycles, and the corresponding response curve confirmed excellent reproducibility, which enabled its reliable application.

We also tested the sensitivity of the porous and dense CuNW aerogel sensors. The CuNW aerogel sensors with different density displayed distinct pressure-sensing curves, as seen in Figure 6a. The porous aerogel sensor exhibited the highest sensitivity (0.7 kPa^{-1}), which to our best knowledge was superior to other reported aerogel-type piezoresistive sensors,[20,23,37] including the highly sensitive polypyrrole/silver aero-sponges design sensor (0.33 kPa^{-1}).[20] In contrast, the dense CuNW aerogel sensor had the lowest sensitivity (0.02 kPa^{-1}), which was nearly 1 order of magnitude lower than the porous CuNW aerogel. The detection limits of the three samples with different microstructure were extracted from Figure 6a as a comparison, as seen in Figure 6b, we further found that the detection limit of the porous aerogel sensor (14 Pa) was lower than that of the dense one (43 Pa), which corresponded to the sensitivity results.

The pressure sensing capability of the CuNW aerogels comes from the pores inside the aerosol. For the porous CuNW aerogel, the rich pores are generated within the bulk aerogel from two contributions: For one thing, vacancies remained within the porous 3-dimensional structure in the process of building the flocs assembled from CuNWs. For another, when flocs stacked further into bulk hydrogel, the loose stacking inevitably leads to pores in between the neighboring flocs (Figure 6c). When the compressive pressure is imposed on the aerogel, the pores generated from the two reasons mentioned above were compressed first to increase the contacting positions in between CuNWs. The number of contacting positions among nanowires was increased as the pressure increased. Simultaneously, the pores existing between the flocs

are also compressed also increased the contacting area in between the flocs. Because of the synergistic effect of these two parts, the resistance of the aerogel monolith under the pressure shows an overall decline. However, for aerogels with dense structure, the absence of pores between the secondary flocs resulted in larger density. So the pressure-induced current only came from tighter connection between the nanowires, which resulted in smaller sensing current increment than porous CuNW aerogel under a certain pressure. The sensitivity of the mixed aerogel was between those of the porous and dense aerogel because the top half of the mixed aerogel was porous structure and the bottom half was dense structure. The comparison of densities (4.3−7.5 mg cm^{-3}) and sensitivities (0.02−0.7 kPa^{-1}) of the all three samples was shown in Figure S4. It was obvious that the sensitivity of the aerogel pressure sensor was related to its density and internal structure. In this way, we could obtain CuNW aerogel-based pressure sensors with tunable sensing properties through adjusting the microstructure of the aerogels in the process of CuNW hydrogel formation.

3. CONCLUSIONS

In summary, we have successfully fabricated CuNW aerogel monolith with different densities and pore structures by adjusting the reaction parameters. A fabrication called "bubbles controlled assembly" was proposed and based on this mechanism the controllability of CuNW aerogel preparation was realized. This fabrication method provides a potential route for the synthesis of other metal nanowires aerogel. Furthermore, fabricated CuNW aerogel monolith was applied as flexible pressure sensors, and the influence of density and pore structure on the sensor sensitivity and detection limit was explored, based on which an aerogel flexible pressure sensor with high sensitivity of 0.7 kPa^{-1} was fabricated. The as-prepared CuNW aerogel pressure sensor possesses a combination of excellent properties, including lightweight, facile fabrication, and high sensitivity, which is highly suitable for the potential application as electronic skins, wearable electronic devices, and other devices.

4. EXPERIMENTAL SECTION

Material. Ethylenediamine (EDA, ≥ 99.0), hydrazine solution (N$_2$H$_4$, 35 wt % in H$_2$O), Sodium hydroxide (NaOH, ≥ 99.5%) were purchased from Sinopharm Chemical Reagent Co., Ltd. Copper(II) sulfate pentahydrate (CuSO$_4$·5H$_2$O, ≥ 99%) was obtained from Alfa Aesar, Silver conductive paint SCP were purchased from Electrolube. All of these chemicals were used as received.

Synthesis of CuNW Aerogel Monolith with Tunable Pore Structure. CuNW hydrogels were prepared by the one-pot method, described briefly as follows: 0.25 mL of CuSO$_4$ (0.5, 1, 1.2 M) was added to 30 mL of NaOH (8, 16 M), and the solution was stirred. After the solution cooled to room temperature, 0.375 mL (or 187.5, 450) EDA (99 wt %) and 0.03 mL (or 0.015, 0.0375) of hydrazine (35 wt %) were added sequentially to the solution. Then, the mixed solution was sonicated for 15 min until it appeared homogeneously milky white. Next, the solution was added to a flat-bottom glass reactor (capacity of 20 mL) with a piece of PU foam placed on top of the liquid surface and was heated at 80 °C for 1 h in oil bath. The product was washed by 5% hydrazine for several times, and then frozen. After that, the CuNW hydrogel monolith was freeze-dried to obtain the aerogel which retained the original shape.

Fabrication of the CuNW Aerogel-Based Pressure Sensor. The aerogel monoliths were assembled into a resistive-type pressure sensor by sandwiching them between a nickel tablets and an aluminum

foil. Aerogel monolith was bonded with electrodes by silver conductive paint and the copper wires were used to form the circuit.

Characterization. The micromorphology characterization of the CuNW was accomplished with a field-emission scanning electron microscopy (Hitachi S-4800). X-ray diffraction (XRD) was carried out on D/max 2550 V X-ray diffraction-meter with Cu−Kα at λ = 1.5406. CuNW hydrogels were freeze-dried by Scientz-10N freeze-dryer. I-t curves in real time of the sensor were measured using an electrochemical workstation (PARSTAT2273, Princeton Applied Research). The force applied on the sensor was detected by force gauge (Mark-10 force gauge, M4−012). The sensitivity and durability of the aerogel monoliths were measured by a high precision electronic universal testing machine (CMT6103, MTS Systems (China) Co., Ltd.) and force gauge. The force (F) and current (I) were recorded. Here, the pressure (P) was calculated by $P = F/A$, where A is the forced area.

■ ASSOCIATED CONTENT

ⓢ Supporting Information

The Supporting Information is available free of charge on the ACS Publications website at DOI: 10.1021/acsami.7b02087.

> XRD patterns of CuNW aerogel. The density of CuNW aerogel obtained from different reaction conditions and reaction temperature. The dependence of the CuNW aerogel density and sensitivity on the internal structure (PDF)

■ AUTHOR INFORMATION

Corresponding Authors

*E-mail: wangranran@mail.sic.ac.cn.
*E-mail: jingsun@mail.sic.ac.cn.

ORCID ⓘ

Jing Sun: 0000-0003-1101-1584

Author Contributions

The manuscript was written through contributions of all authors. All authors have given approval to the final version of the manuscript.

Notes

The authors declare no competing financial interest.

■ ACKNOWLEDGMENTS

■ REFERENCES

(1) Aleman, J.; Chadwick, A. V.; He, J.; Hess, M.; Horie, K.; Jones, R. G.; Kratochvil, P.; Meisel, I.; Mita, I.; Moad, G.; Penczek, S.; Stepto, R. F. T. Definitions of terms relating to the structure and processing of sols, gels, networks, and inorganic-organic hybrid materials (IUPAC Recommendations 2007). *Pure Appl. Chem.* **2007**, *79* (10), 1801−1827.

(2) Dai, S.; Ju, Y. H.; Gao, H. J.; Lin, J. S.; Pennycook, S. J.; Barnes, C. E. Preparation of silica aerogel using ionic liquids as solvents. *Chem. Commun.* **2000**, *3*, 243−244.

(3) Morris, C. A.; Anderson, M. L.; Stroud, R. M.; Merzbacher, C. I.; Rolison, D. R. Silica sol as a nanoglue: Flexible synthesis of composite aerogels. *Science* **1999**, *284* (5414), 622−624.

(4) Dutoit, D. C. M.; Schneider, M.; Baiker, A. Titania-Silica Mixed Oxides 0.1. Influence of Sol-Gel and Drying Conditions on Structural-Properties. *J. Catal.* **1995**, *153* (1), 165−176.

(5) Cognard, G.; Ozouf, G.; Beauger, C.; Berthome, G.; Riassetto, D.; Dubau, L.; Chattot, R.; Chatenet, M.; Maillard, F. Benefits and limitations of Pt nanoparticles supported on highly porous antimony-doped tin dioxide aerogel as alternative cathode material for proton-exchange membrane fuel cells. *Appl. Catal., B* **2017**, *201*, 381−390.

(6) Khalily, M. A.; Eren, H.; Akbayrak, S.; Susapto, H. H.; Biyikli, N.; Ozkar, S.; Guler, M. O. Facile Synthesis of Three-Dimensional Pt-TiO2 Nano-networks: A Highly Active Catalyst for the Hydrolytic Dehydrogenation of Ammonia-Borane. *Angew. Chem., Int. Ed.* **2016**, *55* (40), 12257−12261.

(7) Kobayashi, Y.; Saito, T.; Isogai, A. Aerogels with 3D Ordered Nanofiber Skeletons of Liquid-Crystalline Nanocellulose Derivatives as Tough and Transparent Insulators. *Angew. Chem., Int. Ed.* **2014**, *53* (39), 10394−10397.

(8) Aulin, C.; Netrval, J.; Wagberg, L.; Lindstrom, T. Aerogels from nanofibrillated cellulose with tunable oleophobicity. *Soft Matter* **2010**, *6* (14), 3298−3305.

(9) Xu, Y. X.; Sheng, K. X.; Li, C.; Shi, G. Q. Self-Assembled Graphene Hydrogel via a One-Step Hydrothermal Process. *ACS Nano* **2010**, *4* (7), 4324−4330.

(10) Zhao, J. P.; Ren, W. C.; Cheng, H. M. Graphene sponge for efficient and repeatable adsorption and desorption of water contaminations. *J. Mater. Chem.* **2012**, *22* (38), 20197−20202.

(11) Liang, H. W.; Guan, Q. F.; Chen, L. F.; Zhu, Z.; Zhang, W. J.; Yu, S. H. Macroscopic-Scale Template Synthesis of Robust Carbonaceous Nanofiber Hydrogels and Aerogels and Their Applications. *Angew. Chem., Int. Ed.* **2012**, *51* (21), 5101−5105.

(12) Pierre, A. C.; Pajonk, G. M. Chemistry of aerogels and their applications. *Chem. Rev.* **2002**, *102* (11), 4243−4265.

(13) Koebel, M.; Rigacci, A.; Achard, P. Aerogel-based thermal superinsulation: an overview. *J. Sol-Gel Sci. Technol.* **2012**, *63* (3), 315−339.

(14) Liu, Z. H.; Ding, Y. D.; Wang, F.; Deng, Z. P. Thermal insulation material based on SiO2 aerogel. *Constr Build Mater.* **2016**, *122*, 548−555.

(15) Frackowiak, E.; Beguin, F. Carbon materials for the electrochemical storage of energy in capacitors. *Carbon* **2001**, *39* (6), 937−950.

(16) Zhao, Y.; Liu, J.; Hu, Y.; Cheng, H. H.; Hu, C. G.; Jiang, C. C.; Jiang, L.; Cao, A. Y.; Qu, L. T. Highly Compression-Tolerant Supercapacitor Based on Polypyrrole-mediated Graphene Foam Electrodes. *Adv. Mater.* **2013**, *25* (4), 591−595.

(17) Saliger, R.; Fischer, U.; Herta, C.; Fricke, J. High surface area carbon aerogels for supercapacitors. *J. Non-Cryst. Solids* **1998**, *225* (1), 81−85.

(18) Zhang, Q.; Chung, I.; Jang, J. I.; Ketterson, J. B.; Kanatzidis, M. G. Chalcogenide Chemistry in Ionic Liquids: Nonlinear Optical Wave-Mixing Properties of the Double-Cubane Compound [Sb7S8Br2]-(AlCl4)(3). *J. Am. Chem. Soc.* **2009**, *131* (29), 9896−9897.

(19) Qiu, L.; Liu, J. Z.; Chang, S. L. Y.; Wu, Y. Z.; Li, D. Biomimetic superelastic graphene-based cellular monoliths. *Nat. Commun.* **2012**, *3*, 1241.

(20) He, W. N.; Li, G. Y.; Zhang, S. Q.; Wei, Y.; Wang, J.; Li, Q. W.; Zhang, X. T. Polypyrrole/Silver Coaxial Nanowire Aero-Sponges for Temperature-Independent Stress Sensing and Stress-Triggered Joule Heating. *ACS Nano* **2015**, *9* (4), 4244−4251.

(21) Gong, S.; Cheng, W. One-Dimensional Nanomaterials for Soft Electronics. *Advanced Electronic Materials* **2017**, *3* (3), 1600314.

(22) Tang, Y.; Gong, S.; Chen, Y.; Yap, L. W.; Cheng, W. L. Manufacturable Conducting Rubber Ambers and Stretchable Conductors from Copper Nanowire Aerogel Monoliths. *ACS Nano* **2014**, *8* (6), 5707−5714.

(23) Qin, Y. Y.; Peng, Q. Y.; Ding, Y. J.; Lin, Z. S.; Wang, C. H.; Li, Y.; Li, J. J.; Yuan, Y.; He, X. D.; Li, Y. B. Lightweight, Superelastic, and Mechanically Flexible Graphene/Polyimide Nanocomposite Foam for Strain Sensor Application. *ACS Nano* **2015**, *9* (9), 8933−8941.

(24) Sheng, L. Z.; Liang, Y.; Jiang, L. L.; Wang, Q.; Wei, T.; Qu, L. T.; Fan, Z. J. Bubble-Decorated Honeycomb-Like Graphene Film as Ultrahigh Sensitivity Pressure Sensors. *Adv. Funct. Mater.* **2015**, *25* (41), 6545−6551.

(25) Qiu, L.; Coskun, M. B.; Tang, Y.; Liu, J. Z.; Alan, T.; Ding, J.; Truong, V. T.; Li, D. Ultrafast Dynamic Piezoresistive Response of Graphene-Based Cellular Elastomers. *Adv. Mater.* **2016**, *28* (1), 194.

(26) Hu, H.; Zhao, Z. B.; Wan, W. B.; Gogotsi, Y.; Qiu, J. S. Polymer/Graphene Hybrid Aerogel with High Compressibility, Conductivity, and ″Sticky″ Superhydrophobicity. *ACS Appl. Mater. Interfaces* **2014**, *6* (5), 3242−3249.

(27) Jung, S.; Kim, J. H.; Kim, J.; Choi, S.; Lee, J.; Park, I.; Hyeon, T.; Kim, D. H. Reverse-Micelle-Induced Porous Pressure-Sensitive Rubber for Wearable Human-Machine Interfaces. *Adv. Mater.* **2014**, *26* (28), 4825.

(28) Ge, J.; Yao, H. B.; Wang, X.; Ye, Y. D.; Wang, J. L.; Wu, Z. Y.; Liu, J. W.; Fan, F. J.; Gao, H. L.; Zhang, C. L.; Yu, S. H. Stretchable Conductors Based on Silver Nanowires: Improved Performance through a Binary Network Design. *Angew. Chem., Int. Ed.* **2013**, *52* (6), 1654−1659.

(29) Hammock, M. L.; Chortos, A.; Tee, B. C. K.; Tok, J. B. H.; Bao, Z. A. 25th Anniversary Article: The Evolution of Electronic Skin (E-Skin): A Brief History, Design Considerations, and Recent Progress. *Adv. Mater.* **2013**, *25* (42), 5997−6037.

(30) Tamon, H.; Ishizaka, H.; Mikami, M.; Okazaki, M. Porous structure of organic and carbon aerogels synthesized by sol-gel polycondensation of resorcinol with formaldehyde. *Carbon* **1997**, *35* (6), 791−796.

(31) Tillotson, T. M.; Gash, A. E.; Simpson, R. L.; Hrubesh, L. W.; Satcher, J. H.; Poco, J. F. Nanostructured energetic materials using sol-gel methodologies. *J. Non-Cryst. Solids* **2001**, *285* (1−3), 338−345.

(32) Eberle, A. P. R.; Baird, D. G.; Wapperom, P. Rheology of non-Newtonian fluids containing glass fibers: A review of experimental literature. *Ind. Eng. Chem. Res.* **2008**, *47* (10), 3470−3488.

(33) Jung, S. M.; Jung, H. Y.; Dresselhaus, M. S.; Jung, Y. J.; Kong, J., A facile route for 3D aerogels from nanostructured 1D and 2D materials. *Sci. Rep.* **2012**, *2*, DOI: 10.1038/srep00849.

(34) Jung, S. M.; Preston, D. J.; Jung, H. Y.; Deng, Z.; Wang, E. N.; Kong, J. Porous Cu Nanowire Aerosponges from One-Step Assembly and their Applications in Heat Dissipation. *Adv. Mater.* **2016**, *28* (7), 1413−9.

(35) Tang, Y.; Yeo, K. L.; Chen, Y.; Yap, L. W.; Xiong, W.; Cheng, W. L. Ultralow-density copper nanowire aerogel monoliths with tunable mechanical and electrical properties. *J. Mater. Chem. A* **2013**, *1* (23), 6723−6726.

(36) Chang, Y.; Lye, M. L.; Zeng, H. C. Large-scale synthesis of high-quality ultralong copper nanowires. *Langmuir* **2005**, *21* (9), 3746−3748.

(37) Yao, H. B.; Ge, J.; Wang, C. F.; Wang, X.; Hu, W.; Zheng, Z. J.; Ni, Y.; Yu, S. H. A flexible and highly pressure-sensitive graphene-polyurethane sponge based on fractured microstructure design. *Adv. Mater.* **2013**, *25* (46), 6692−8.